Title

Cryo-electron microscopy studies of empty capsids of human parvovirus B19 complexed with its cellular receptor.

Journal

Proceedings of the National Academy of Sciences of the United States of America, 93(15)

ISSN

0027-8424

Authors

Chipman, PR
Agbandje-McKenna, M
Kajigaya, S
et al.

Publication Date

1996-07-23

DOI

10.1073/pnas.93.15.7502

Peer reviewed

Proc. Natl. Acad. Sci. USA
Vol. 93, pp. 7502–7506, July 1996
Biochemistry

Cryo-electron microscopy studies of empty capsids of human parvovirus B19 complexed with its cellular receptor

PAUL R. CHIPMAN*, MAVIS AGBANDJE-MCKENNA*†, SACHIKO KAJIGAYA‡, KEVIN E. BROWN‡, NEAL S. YOUNG‡, TIMOTHY S. BAKER*, AND MICHAEL G. ROSSMANN*§

*Department of Biological Sciences, Purdue University, West Lafayette, IN 47907-1392; and ‡National Heart, Lung and Blood Institute, Building 10, Room 7C103, National Institutes of Health, Bethesda, MD 20892

Contributed by Michael G. Rossmann, April 19, 1996

ABSTRACT **The three-dimensional structures of human parvovirus B19 VP2 capsids, alone and complexed with its cellular receptor, globoside, have been determined to 26 Å resolution. The B19 capsid structure, reconstructed from cryo-electron micrographs of vitrified specimens, has depressions on the icosahedral 2-fold and 3-fold axes, as well as a canyon-like region around the 5-fold axes. Similar results had previously been found in an 8 Å resolution map derived from x-ray diffraction data. Other parvoviral structures have a cylindrical channel along the 5-fold icosahedral axes, whereas density covers the 5-fold axes in B19. The glycolipid receptor molecules bind into the depressions on the 3-fold axes of the B19:globoside complex. A model of the tetrasaccharide component of globoside, organized as a trimeric fiber, fits well into the difference density representing the globoside receptor. Escape mutations to neutralizing antibodies map onto the capsid surface at regions immediately surrounding the globoside attachment sites. The proximity of the antigenic epitopes to the receptor site suggests that neutralization of virus infectivity is caused by preventing attachment of viruses to cells.**

Parvovirus B19 is the only member of *Parvoviridae* pathogenic to man (1, 2). Acute infection causes a childhood measles-like rash condition, erythrema infectosium, also known as fifth disease, and acute or chronic arthritis in adults. In persons with underlying hemolysis, acute B19 infection results in transient aplastic crises, due to cessation in red blood cell production, which is caused by tropism of B19 to erythroid progenitor cells. In immunocompromised individuals, such as AIDS patients and patients undergoing immunosuppressive drug therapy, persistent B19 infection causes chronic severe anemia due to erythroid marrow failure. B19 infection of pregnant women may cause hydrops fetalis (congestive heart failure) of the fetus and spontaneous abortions due to the inability of the fetus to mount an adequate immune response.

Parvoviruses have a single-stranded DNA genome encapsidated in a $T = 1$ (60 structurally equivalent subunits) icosahedral protein capsid, approximately 260 Å in diameter. The major structural protein, VP2, has a molecular mass of 58,000 and consists of an eight-stranded, anti-parallel, β-barrel motif (with β strands B, C, . . . , I), similar to that found in many other viral capsid proteins (3). This β-barrel structure contains only about one-third of the amino acid content in each polypeptide and lies mostly below the capsid surface, which is formed by large insertions between the β-strands. For canine parvovirus (CPV) (4) and feline panleukopenia virus (FPV) (5), the loops between the B and C (loop 1), E and F (loop 2), and G and H (loops 3 and 4) β-strands contain 36, 74, and 223 residues, respectively. These loops form most of the capsid surface, with loops 3 and 4 forming the bulk of the spikes that extend 22 Å radially outwards around the 3-fold axes. The insertion of 20 amino acids between the D and E strands forms an anti-parallel β-ribbon, which, together with similar insertions in the other 5-fold-related polypeptides, forms a cylindrical structure about each 5-fold axis. A canyon-like depression encircles each of the 5-fold axes and a dimple-like depression occurs at each 2-fold axis. In CPV and FPV, one in five of the capsid proteins has its amino ends externalized by being threaded through the channel along the 5-fold icosahedral axes.

For B19, the major capsid protein (VP2) makes up about 95% of the viral capsid. VP2 lacks 226 "unique" amino terminal residues compared with the minor capsid protein (VP1). The crystal structure of empty particles of B19 produced in a baculovirus expression system (6) has been determined to 8 Å resolution (7). These capsids, which contain both VP1 and VP2 or VP2 alone, are indistinguishable from the native empty capsids both antigenically and in electron micrographs of negatively-stained specimens (6, 8). The electron density (7) and a sequence alignment (9) showed that the surface features of B19 differ greatly from those of CPV and FPV. In particular, the spikes on the 3-fold vertices are missing in B19. Another major difference is that the channels along the 5-fold axes appear to be closed at the surface in B19. However, the central β-barrel domain remains substantially unchanged.

The initiation of viral replication for parvoviruses requires interactions with specific cell surface receptors. Brown *et al.* (10) have shown that one of the blood group P antigens, the glycolipid globoside (≈1400 daltons), is the receptor for B19. Erythrocytes that contain globoside hemagglutinate in the presence of B19, *in vitro* (10, 11). Some parvoviruses, such as CPV (12) and minute virus of mouse (13), use carbohydrates for cellular attachment. Furthermore, CPV and FPV bind to glycolipids that have a structure similar to P antigens (Y. Suzuki, personal communication). Globoside is also found in endothelial cells, which may be the site of B19 replication resulting in fifth disease (14). The presence of globoside in fetal cardiac myocytes may lead to B19 infection and myocarditis (15, 16).

The structure of human rhinovirus 14 complexed to its receptor molecule, intercellular adhesion molecule-1, a membrane-bound glycoprotein (17), and the structures of influenza virus and polyoma virus complexed with analogues of the carbohydrate moiety of their receptors have been reported (18–20). We report here the use of cryo-electron microscopy (cryo-EM) and three-dimensional image analysis of B19 empty capsids, alone and complexed with globoside.

MATERIALS AND METHODS

The B19 empty particles consisting only of VP2, produced in a baculovirus expression system, were propagated and purified

The publication costs of this article were defrayed in part by page charge payment. This article must therefore be hereby marked "*advertisement*" in accordance with 18 U.S.C. §1734 solely to indicate this fact.

Abbreviations: CPV, canine parvovirus; FPV, feline panleukopenia virus; cryo-EM, cryo-electron microscopy.

†Present address: Department of Biological Sciences, University of Warwick, Coventry, CV4 7AL, United Kingdom.
§To whom correspondence should be addressed.

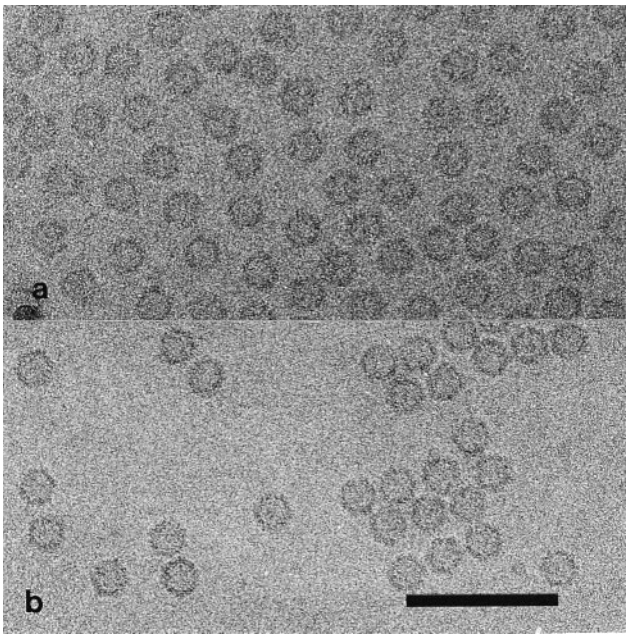

FIG. 1. Cryo-EM images of (*a*) unstained, frozen-hydrated B19 empty particles and (*b*) B19 complexed with globoside. (Scale bar = 1000 Å.)

as reported (6). The empty capsids were prepared for cryo-EM in 10 mM Tris·HCl (pH 7.5), at a concentration of 2.7 mg/ml. The B19:globoside complex was formed by incubation of B19 with globoside at 0.11 mg/ml, in the same buffer with 1.0% dimethyl sulfuoxide (DMSO), for approximately 16 hr at 4°C. Cryo-EMs of B19 VP2 capsids and the B19:globoside complex were recorded at a defocus level of approximately 0.8 μm and an irradiation level of $\approx$18 electrons/Å^2 (Fig. 1). There were no visible differences between the particles without or with bound receptor. This finding contrasts with the decoration of rhinovirus with its much larger (25 kDa) bound receptor fragments, which are clearly visible in unprocessed images

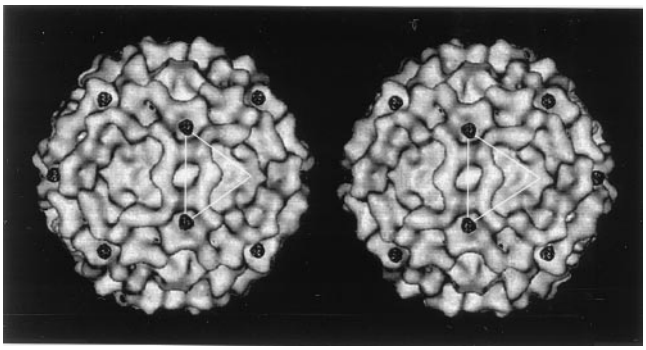

FIG. 3. A stereoscopic view of the difference map between B19 complexed with the globoside receptor and B19 on its own superimposed onto the B19 cryo-EM reconstructed surface image. Globoside molecules bind into the surface depressions at the 3-fold vertices. The triangle outlines one icosahedral asymmetric unit.

(17). Thirty-seven images of the B19 VP2 particles were combined to calculate a three-dimensional reconstruction (Fig. 2 *c* and *d*) to a resolution of at least 26 Å (21–24). The three-dimensional reconstruction of the complex (Fig. 2 *e* and *f*) was calculated in the same manner from 17 particles at the same resolution. A difference map (Fig. 3) between the complex and B19 capsids was calculated after scaling of the densities to optimize the radial dimensions and average density levels (25).

RESULTS AND DISCUSSION

The reconstructed cryo-EM density map of the B19 VP2 capsid shows depressions at both the icosahedral 2-fold and 3-fold axes and canyon-like regions about each of the 5-fold axes (Fig. 2 *c* and *d*) consistent with the earlier 8 Å resolution x-ray map (7). Unlike CPV (Fig. 2 *a* and *b*), B19 (Fig. 2 *c* and *d*) lacks a channel at the 5-fold icosahedral axes. The reconstructed map of the B19:globoside complex (Fig. 2 *e* and *f*) showed extra density on the 3-fold depression when compared with the B19 VP2 capsid alone. A difference map between the

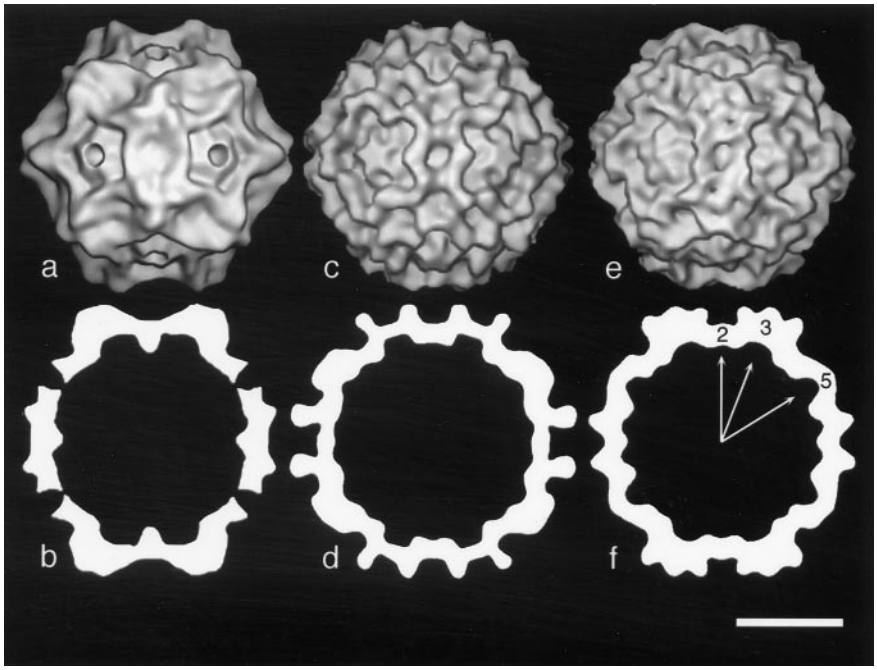

FIG. 2. The structure of CPV (21 Å resolution) derived from x-ray crystallography (*a* and *b*) is compared with image reconstructions of B19 (*c* and *d*) and the B19:globoside complex with its receptor (*e* and *f*). Surface views are shown in *a*, *c*, and *e* and central sections are shown in *b*, *d*, and *f*. Small differences can also be seen at the 5-fold axes. (Scale bar = 100 Å.)

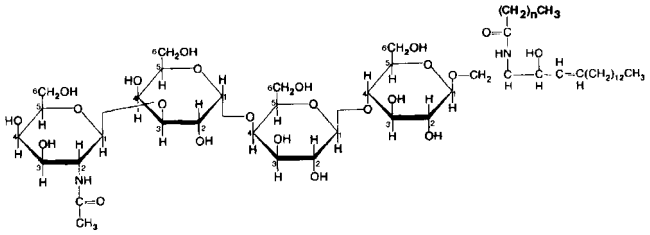

FIG. 4. Globoside, (Gal-*N*-Ac)(β1-3)Gal(α1-4)Gal(β1-4)Glc-Cer, where Gal-*N*-Ac is *N*-acetylgalactosamine, Gal is galactose, Glc is glucose, Cer is ceramide, and n = 16, 18, 22, or 24.

complex and B19 VP2 capsid (Fig. 3) showed that the receptor molecules bind into the depression at the icosahedral 3-fold axes. The globoside density extends approximately 19 Å out from the surface of the depression. Small differences can also be seen around the 5-fold axes (compare Fig. 2 *d* and *f*). These may indicate conformational changes as a result of globoside binding, but more probably represent noise as a consequence of the fewer number of particles used in the image reconstruction of the complex. The height of the globoside was 4.5σ and the height of the features about the 5-fold axes was 2σ above the backgound, where σ was the root-mean-square deviation from zero of the electron density in the difference map.

The volume of the roughly spherical globoside difference density attributed to globoside is approximately 3600 Å^3, as determined at a contour level just above the noise of the map. Assuming a density of about 1.1 gm/cm^3 for a glycolipid, this volume would be occupied by three molecules each having a mass of 655 Da (26). The interaction of the receptor with the capsid mainly involves the sugar portion of the glycolipid, as has been observed for other viruses that use glycolipids or glycoproteins as receptor molecules (18–20). The mass of the carbohydrate component of globoside is 690 Da, which gives a reasonable fit to the 655 Da expected to fill the difference electron density. Thus, the lipid component of globoside (Fig. 4) is likely to be disordered and, therefore, not visible in the density map.

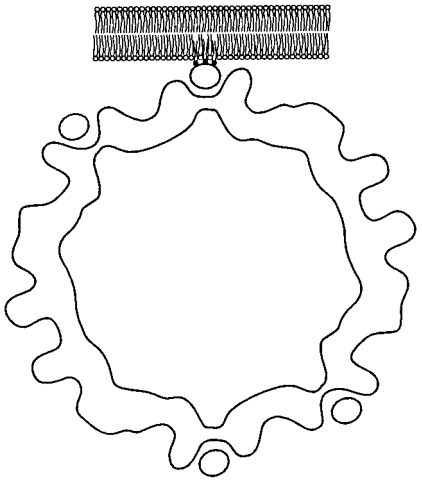

FIG. 6. Schematic representation of the docking of B19 to a cellular receptor membrane glycolipid.

The segment having the sequence Glc(β1-3)Glc(β1-3)Glc(β1-3)Glc(β1-3), as observed in the naturally occurring triple helical fiber structure of 1-3-β-D glucan (27), was used as the tetrasaccharide model to fit into the difference map. This structure has a rise per residue of 2.94 Å. Every sugar residue has the OH group at the C_2 position facing the 3-fold axis, forming a hydrogen bond with a 3-fold-related helical counterpart. The (β1-3) linkage between the first and second sugar residues of globoside is the same as in the glucan segment. The only possible adjustments were a rotation about and a small translation along the 3-fold axis, which were needed to make a hydrophobic contact with Tyr401 of B19 VP2. Similar hydrophobic contacts between sugar and aromatic residues are common features of protein–carbohydrate interactions (28, 29). The resulting fit of this trimeric tetrasac-

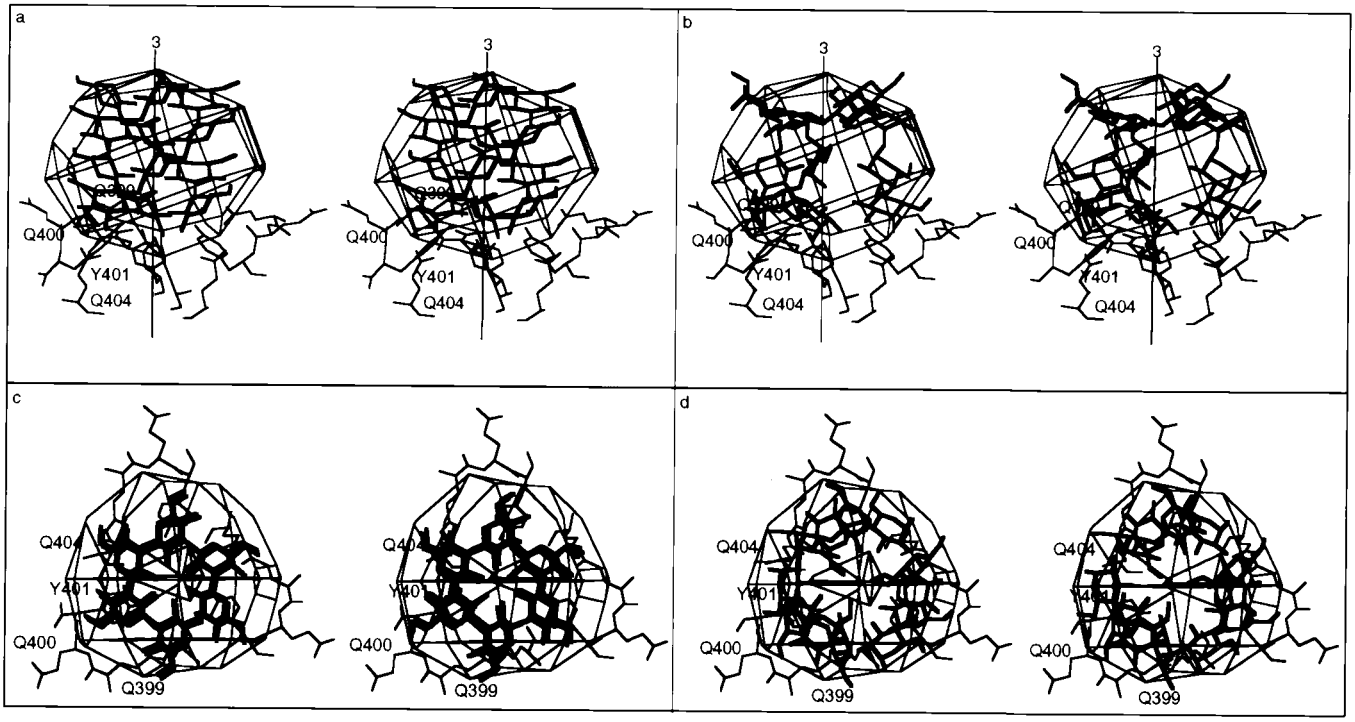

FIG. 5. Fit of tetrasaccharide trimers (thick lines) into the receptor difference density. Fit of the 1-3-β-D glucan fiber structure, which has a (β1-3) linkage between successive glucose moieties (*a* and *c*) and of the preferred structure of the globoside carbohydrate moiety positioned as suggested by the glucan fiber structure (*b* and *d*). *a* and *b* are side views (perpendicular to the icosahedral 3-fold axis); *c* and *d* are views down the 3-fold axis.

```
                    <--------loop 2------->
  Canine    208 WRYYFQWDRTL..IPSHTGTSGT..PTNIYHGTD 237
Human_B19   194 YAYL.......TV..GDVNT...QGISGDSKKLA 205

                  <--------------loop 4-------------->
  Canine    407 GRYPEGDWIQNINFNLPVTNDNVLLPTDPIGGKTGINYT 445
Human_B19   384 LQGLNMHTY........FPNKGTQQYTD.........YT 402
```

FIG. 7. Modified sequence alignment (9) of CPV to B19 in the loop 2 and 4 regions. The large insertions in loop 2 and loop 4 form a small spike on each 3-fold axis in CPV. Conversely, the deletions in B19 leave a slight depression on the 3-fold axes.

charide is fully consistent with the difference electron density map (Fig. 5 *a* and *c*).

The probable structure of the globoside carbohydrate (Fig. 4) was predicted from the allowed dihedral angles for each linkage and the most stable chair conformation of the monosaccharides (30, 31). The principal difference between the carbohydrate moiety of globoside and that of the glucan structure arises at the (α1-4) linkage between the second and third sugar residues, giving the globoside tetrasaccharide a kink at this junction. Its first two sugars were superimposed onto the first two residues of the glucan triple helix. Only a small adjustment was required to avoid steric interference around the 3-fold axis. In the model, the O_6 atom of the third sugar residue faces the 3-fold axis where it will make a hydrogen bond with a 3-fold-related molecule. This fit (Fig. 5 *b* and *d*) leaves the ceramide extending outwards, presumably able to anchor into the cellular membrane. The trimeric lipid arrangement is likely to be incorporated into the usual hexagonal packing of lipid bilayers (Fig. 6).

An attempt to model the B19 structure based on that of CPV and FPV used the 8 Å resolution B19 map as a constraint. The atomic structure of CPV was modified in two ways; (*a*) to be consistent with the aligned B19 sequence (9) by substituting individual residues and (*b*) the CPV insertions that are absent in B19 were removed according to a modified alignment scheme (Fig. 7). The footprint of the trimeric receptor on the viral surface is shown in Fig. 8. The depression at the icosahedral 3-fold axes has a hydrophobic center (including Tyr-401) that is surrounded by polar residues within the asymmetric unit of the globoside footprint.

Monoclonal antibodies mAb E, L, and 521-5D are known to inhibit hemagglutination of B19 (11). The epitopes of these mAbs have been associated with residues 57–77, 345–365, and 446–466 of B19 VP2, respectively (2). Segments of these peptides are on the viral surface as shown on the surface roadmap (Fig. 8). mAbs E and L bind within 10 Å of the globoside attachment site. As B19 binds to erythrocytes, inhibition of hemagglutination suggests that these mAbs may also inhibit infection. Thus, these antibodies, which have a footprint of at least 34 Å diameter (32), might inhibit hemagglutination by receptor blocking.

The relationship between the receptor attachment site within a surface depression at the 3-fold axes of B19 surrounded by neutralization epitopes is analogous to depressions found on the surfaces of rhinoviruses (33), polioviruses (34),

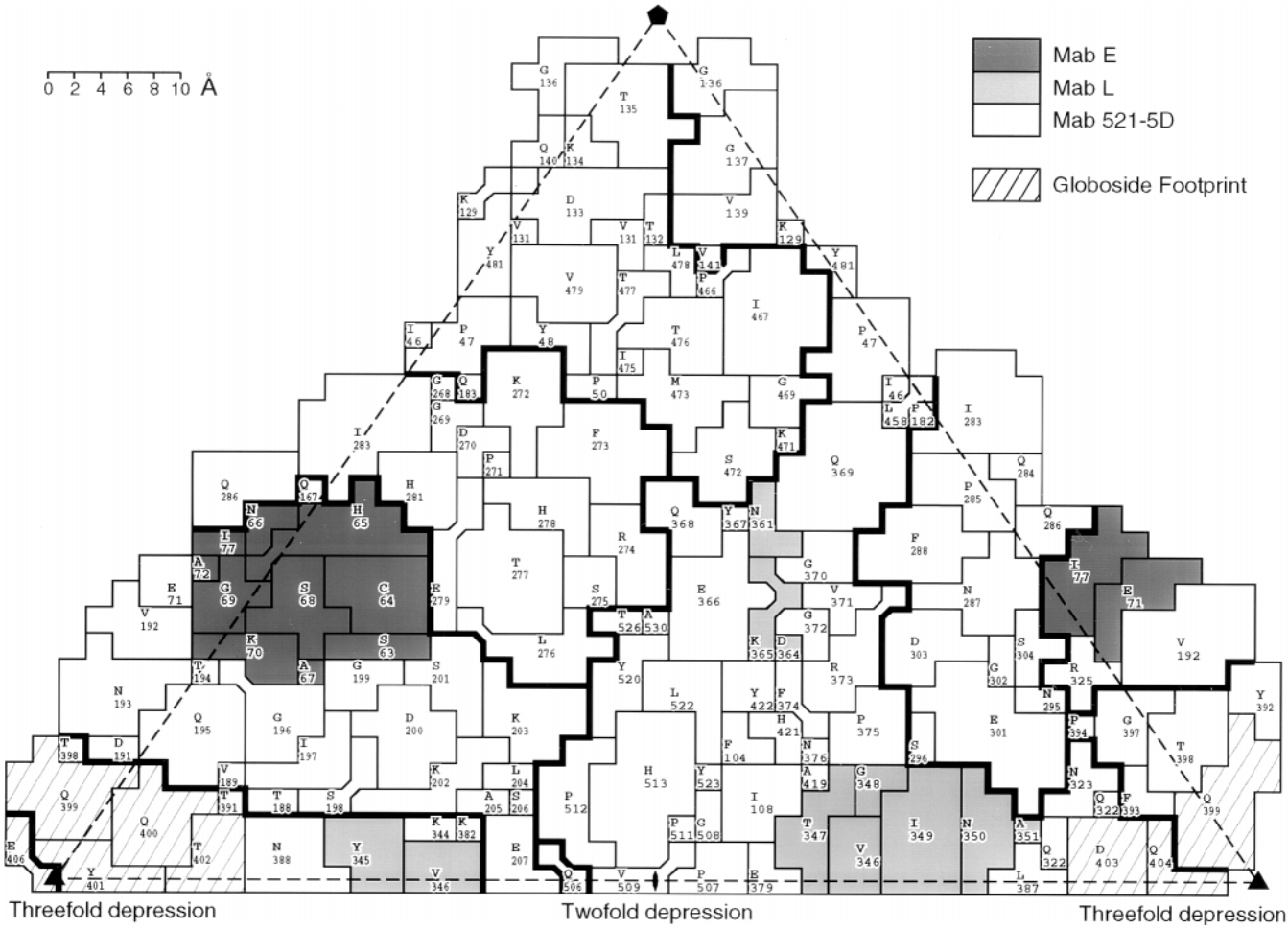

FIG. 8. A "roadmap" of one icosahedral asymmetric unit showing the surface residues of the B19 virus based on a modified sequence alignment (Fig. 7) relative to CPV. The footprint of the globoside receptor on the viral surface (cross-hatched region) and the site of escape mutations for the neutralizing antibodies mAb E, L, and 521-5D (shaded regions) are shown.

and influenza viruses (20). This arrangement ensures that naturally occurring mutants at the base of the depression can escape host immune surveillance, but recognize and bind to the receptor. The binding of globoside in the icosahedral 3-fold depression has identified the region of the B19 capsid involved in host recognition and binding. It remains to be determined how attachment initiates cell entry and viral transport to the nucleus.

We are grateful to R. Chandrasekaran, V. Reddy, and A. Simpson for help with modeling of the tetrasaccharide component of the globoside receptor. We also thank S. Wilder and C. Towell for help in the preparation of the manuscript. The work was supported by National Science Foundation Grant MCB 9102855 and National Institutes of Health Grant AI 11219 to M.G.R., National Institutes of Health Grant GM 33050 to T.S.B., National Institutes of Health Grant AI 33468 to M.G.R. and C. R. Parrish (Cornell University), and National Institutes of Health Program Project Grant AI 35212 to the Purdue University Virology group.

1. Brown, K. E., Young, N. S. & Liu, J. M. (1994) *Crit. Rev. Oncol. Hematol.* **16,** 1–31.
2. Brown, K. E. (1995) MS thesis (Cambridge University, Cambridge, U.K.).
3. Rossmann, M. G. & Johnson, J. E. (1989) *Annu. Rev. Biochem.* **58,** 533–573.
4. Tsao, J., Chapman, M. S., Agbandje, M., Keller, W., Smith, K., Wu, H., Luo, M., Smith, T. J., Rossmann, M. G., Compans, R. W. & Parrish, C. R. (1991) *Science* **251,** 1456–1464.
5. Agbandje, M., McKenna, R., Rossmann, M. G., Strassheim, M. L. & Parrish, C. R. (1993) *Proteins* **16,** 155–171.
6. Kajigaya, S., Fujii, H., Field, A., Anderson, S., Rosenfeld, S., Anderson, L. J., Shimada, T. & Young, N. S. (1991) *Proc. Natl. Acad. Sci. USA* **88,** 4646–4650.
7. Agbandje, M., Kajigaya, S., McKenna, R., Young, N. S. & Rossmann, M. G. (1994) *Virology* **203,** 106–115.
8. Brown, C. S., Van Lent, J. W. M., Vlak, J. M. & Spaan, W. J. W. (1991) *J. Virol.* **65,** 2702–2706.
9. Chapman, M. S. & Rossmann, M. G. (1993) *Virology* **194,** 491–508.
10. Brown, K. E., Anderson, S. M. & Young, N. S. (1993) *Science* **262,** 114–117.
11. Brown, K. E. & Cohen, B. J. (1992) *J. Gen. Virol.* **73,** 2147–2149.
12. Basak, S., Turner, H. & Parr, S. (1994) *Virology* **205,** 7–16.
13. Crawford, L. V. (1966) *Virology* **29,** 605–612.
14. Rouger, P., Gane, P. & Salmon, C. (1987) *Rev. Fr. Transfus. Immunol.-Hematol.* **30,** 699–708.
15. Naides, S. J. & Weiner, C. P. (1989) *Prenat. Diagn.* **9,** 105–114.
16. Morey, A. L., Patou, G., Myint, S. & Fleming, K. A. (1992) *J. Gen. Virol.* **73,** 3313–3317.
17. Olson, N. H., Kolatkar, P. R., Oliveira, M. A., Cheng, R. H., Greve, J. M., McClelland, A., Baker, T. S. & Rossmann, M. G. (1993) *Proc. Natl. Acad. Sci. USA* **90,** 507–511.
18. Sauter, N. K., Glick, G. D., Crowther, R. L., Park, S.-J., Eisen, M. B., Skehel, J. J., Knowles, J. R. & Wiley, D. C. (1992) *Proc. Natl. Acad. Sci. USA* **89,** 324–328.
19. Stehle, T., Yan, Y., Benjamin, T. L. & Harrison, S. C. (1994) *Nature (London)* **369,** 160–163.
20. Weis, W., Brown, J. H., Cusack, S., Paulson, J. C., Skehel, J. J. & Wiley, D. C. (1988) *Nature (London)* **333,** 426–431.
21. Conway, J. F., Duda, R. L., Cheng, N., Hendrix, R. W. & Steven, A. C. (1995) *J. Mol. Biol.* **253,** 86–99.
22. Fuller, S. D., Butcher, S. J., Cheng, R. H. & Baker, T. S. (1996) *J. Struct. Biol.* **116,** 45–55.
23. Baker, T. S. & Cheng, R. H. (1996) *J. Struct. Biol.* **116,** 120–130.
24. Baker, T. S., Newcomb, W. W., Olson, N. H., Cowsert, L. M., Olson, C. & Brown, J. C. (1991) *Biophys. J.* **60,** 1445–1456.
25. Dryden, K. A., Wang, G., Yeager, M., Nibert, M. L., Coombs, K. M., Furlong, D. B., Fields, B. N. & Baker, T. S. (1993) *J. Cell Biol.* **122,** 1023–1041.
26. Matthews, B. W. (1968) *J. Mol. Biol.* **33,** 491–497.
27. Deslandes, Y., Marchessault, R. H. & Sarko, A. (1980) *Macromolecules* **13,** 1466–1471.
28. Kreusch, A. & Schulz, G. E. (1994) *J. Mol. Biol.* **243,** 891–905.
29. Schirmer, T., Keller, T. A., Wang, Y. & Rosenbusch, J. P. (1995) *Science* **267,** 512–514.
30. Sathyanarayana, B. K. & Rao, V. S. R. (1972) *Biopolymers* **11,** 1379–1394.
31. Sathyanarayana, B. K. & Rao, V. S. R. (1971) *Biopolymers* **10,** 1605–1615.
32. Wikoff, W. R., Wang, G., Parrish, C. R., Cheng, R. H., Strassheim, M. L., Baker, T. S. & Rossmann, M. G. (1994) *Structure* **2,** 595–607.
33. Rossmann, M. G., Arnold, E., Erickson, J. W., Frankenberger, E. A., Griffith, J. P., Hecht, H. J., Johnson, J. E., Kamer, G., Luo, M., Mosser, A. G., Rueckert, R. R., Sherry, B. & Vriend, G. (1985) *Nature (London)* **317,** 145–153.
34. Racaniello, V. R. (1992) *Semin. Virol.* **3,** 473–481.